Preprint, published in *Meccanica*, 2015, **50**(3), 633-647

Dynamic and energy analysis of frictional contact instabilities on a lumped system.

Jacopo Brunetti · Francesco Massi · Walter D'Ambrogio · Yves Berthier

Abstract When dealing with complex mechanical systems, the frictional contact is at the origin of significant changes in their dynamic behavior. The presence of frictional contact can give rise to mode-coupling instabilities that produce harmonic friction induced vibrations. Unstable vibrations can reach large amplitude that could compromise the structural and surface integrity of the system and are often associated with annoying noise emission. The study of this kind of dynamic instability has been the subject of many studies ranging from both theoretical and numerical analysis of simple lumped models to numerical and experimental investigation on real mechanical systems, such as automotive brakes, typically affected by such issue.

In this paper the numerical analysis of a lumped system constituted by several degrees of freedom in frictional contact with a slider is presented, where the introduction of friction can give rise to an unstable dynamic behavior. Two different approaches are used to investigate the effects of friction forces. The first approach, the Complex Eigenvalues Analysis (CEA), allows for calculating the complex eigenvalues of the linear system that can be characterized by a positive real part (i.e. negative modal damping). The complex eigenvalues and eigenvectors of the system are investigated with respect to friction. In the second approach a non linear model has been developed accounting for the stick-slip-detachment behavior at the interface to solve the time history solution and analyze the unstable vibration. The effects of boundary conditions and of system parameters are investigated. Results comparison between the two different approaches highlights how nonlinearities affect the time-history solution. The lumped model allows for a detailed analysis of the energy flows between the boundary and the system during self-excited vibrations, which are at the origin of the selection between the predicted unstable mode.

Keywords frictional contact · mode coupling instability · unstable induced vibration.

J. Brunetti · Y. Berthier
Universite de Lyon, CNRS, INSA-Lyon, LaMCoS UMR 5259,
20 Rue Des Sciences, 69621, Villeurbanne, France
Tel.: +33-
Fax: +123-45-678910
E-mail: jacopo.brunetti@insa-lyon.fr

F. Massi
Universita di Roma La Sapienza, Dip. di Ingegneria Meccanica e Aerospaziale,
via Eudossiana, 18, 00184, Roma, Italy

W. D'Ambrogio · J. Brunetti
Universita dell'Aquila, Dipartimento di Ingegneria Industriale e dell'Informazione e di Economia,
Via G. Gronchi, 18, 67100, L'Aquila (AQ), Italy

1 Introduction

Complex mechanical systems are always subjected to vibrations induced by the frictional contacts [Sheng, 2007; Ibrahim, 1994a,b]. Such vibrations can be either of low amplitude, due to the system response at the broadband noise excited by the irregularities at the contact surface, or characterized by an unstable response of the dynamic system (stick-slip, sprag-slip, mode lock-in) and the consequent large vibration amplitude [Akay, 2002]. The presence of frictional contact can give rise to mode-coupling instabilities that produce harmonic friction induced vibration. Unstable oscillations can reach large amplitude that are generally associated with annoying noise emission [Kinkaid et al, 2003; Massi et al, 2006].

The study of this kind of contact dynamic instability has been the subject of many numerical [Coudeyras et al, 2009; Massi et al, 2007; Cantone and Massi, 2011; Chen and Zhou, 2007; Baillet et al, 2005; Chevillot et al, 2010; Bengisu and Akay, 1994; Ouyang et al, 2005; Dezi et al, 2014] and experimental studies on specific mechanical systems [Renouf et al, 2011; Brunetti et al, 2014], such as automotive brakes [Massi and Giannini, 2008; Giannini and Sestieri, 2006; Kinkaid et al, 2003] or hip endoprosthesis [Weiss

et al, 2012; Fan et al, 2011], that are generally affected by such issue. These works have shown howa Complex Modal Analysis (CEA) can identify the stable and unstable behavior of the system and that the frequency found to be unstable, both experimentally and numerically, is close to one of the unstable modes resulting form the CEA.

Theoretic and numerical analyses of simple lumped models [Hoffmann et al, 2002; Hoffmann and Gaul, 2003; Sinou and Jézéquel, 2007] considered mainly systems with no more than one unstable mode to observe the effect of some parameters on the complex eigenvalues of the system or on the size of the limit cycle of the oscillations.

Often, contact nonlinearities have been replaced by non linear stiffness in order to apply nonlinear resolution methods [Sinou et al, 2004] and find the steady state response of the system and its limit cycle.

By the analysis of the contact behavior of complex mechanical systems it can be observed that the variation of the contact status strongly affects the limit cycle; periodical variations of contact status can be found locally at the contact [Tonazzi et al, 2013; Di Bartolomeo et al, 2012], affecting the maximum amplitude of vibration reached by the mechanical system (limit cycle).

In this paper, the numerical analysis is extended to a lumped system constituted by several degrees of freedom in frictional contact with a slider, where the introduction of friction can give rise to an unstable dynamic behavior. The nonlinear effects of the contact are in this case accounted for by considering the possibility of switching between sliding, sticking and detachment of the bodies in contact, while the springs and dampers linking the different masses have a linear behavior.

The novelty of the presented lumped system is the presence of both "contact" masses directly involved into the contact and "internal" masses, which aren't directly involved into the contact and are representative of the "internal" system/bulk dynamics. By this way the system wants to be more representative, with respect to models into the literature, of complex mechanical systems where the contact interfaces represent only a portion of the whole system. It allows for consider both the dynamic behavior of the system and the local dynamic behavior at the contact interface. These aspects are both fundamental to model and understand friction induced vibrations.

Similar models adopted in literature generally consider just a single mass in contact. This assumption brings to an excessive simplification of the contact interface that is consequently reduced to a single contact point; the distribution of the contact quantities and the transitions among the different contact conditions along the interface are not considered. On the contrary, transient analysis performed on more complex and realistic models, such as finite element models with an extended contact interface, showed an asynchronous transition among the different contact conditions for all the interface nodes and a non-uniform distribution of the contact quantities along the interface. Hence, different nodes of the same contact interface can have different contact status at the same time instant [Tonazzi et al, 2013]. The modularity of the system developed in this work allows for increasing the complexity of the system such as the number of unstable modes; moreover, the increase of the number of contacting masses allows to be more representative of the contact distribution of a continuous contact.

For these reasons the proposed model can be considered as an useful tool for investigating friction induced vibrations of real mechanical systems, such as brake systems or joints, allowing for a finer reproduction of the contact and dynamics response (with respect to classical lumped models).

Two approaches are used to investigate the effects of friction forces. The CEA performed on the system in the initial status allows for calculating the complex eigenvalues of the system that can be characterized by positive real part (i.e. negative apparent modal damping). In case of instabilities (positive real part) the vibration amplitude increases and the system response is unstable. The complex eigenvectors are investigated to discuss the energy flows associated with either stable or unstable modes. In the second approach, a nonlinear model has been developed to account for the actual contact behavior at the interface during the transient response. In this case the transient solution has been computed by modal composition techniques, with the aim to analyze the stable or unstable friction induced vibrations in the modal space.

Thus, the transient response is directly correlated to the results from the CEA performed in all the different statuses reached by the system during the vibration and a detailed energy analysis is performed to better understand the flows of energy during the limit cycle of vibration.

2 Lumped model

The analyzed system is composed by 2 subsystems each one composed by 2 masses. One mass of each subsystem is in contact with a rigid slider with a constant friction coefficient μ. This law, applied locally on each node of finite element models, can reproduce the measured dynamic response of complex systems [Brunetti et al, 2013]. Furthermore, macroscopic effects, such as the variation of the global friction coefficient, can be related more to a variation of the dynamic response of the system than to a local variation of the friction coefficient [Tonazzi et al, 2013].

The slider is inclined at the angle θ and moves with speed v.

In the model formulation, the preload at the contact can be applied either by external forces F_{ex}, applied to the up-

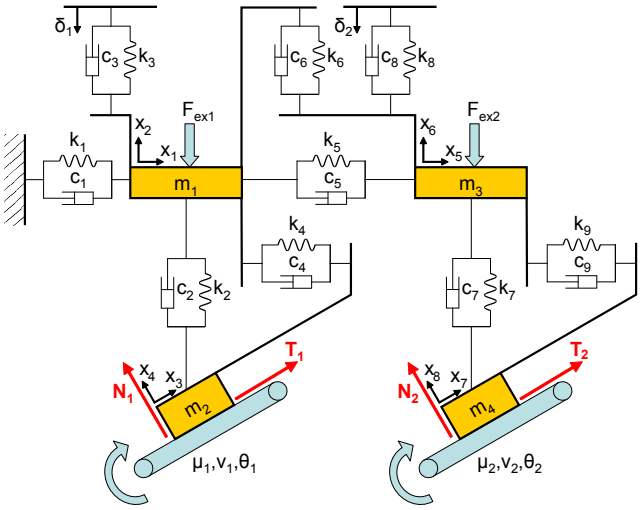

Fig. 1 Lumped system considerd for calculations.

per masses (m_1 and m_3 in Fig. 1), or by displacements δ imposed on the upper constraint.

The contact between the sliders and the lower masses (m_2 and m_4 in Fig. 1) acts as an unilateral constraint ($x_4 \geq 0$ and $x_8 \geq 0$ in Fig. 1) and the reaction forces, in normal (N) and tangential (T) direction, in case of sliding can be expressed as follow:

$$\begin{cases} N > 0, \;\; T \leq -\mu \dfrac{\dot{x}_t - v}{\|\dot{x}_t - v\|} N & \text{if } \; x_n = 0 \\ N = 0, \;\; T = 0 & \text{if } \; x_n > 0 \end{cases} \tag{1}$$

where $\dot{x}_t$ is the speed of the contacting masses in the direction tangential to the contact, x_n is the position in the direction normal to the contact and the positive directions are as in Fig. 1.

To analyze the nonlinear behavior of the system the following status of contact have been considered:

- Positive Sliding ($\dot{x}_t - v < 0$): sliding contact with positive relative speed and negative friction force;
- Negative Sliding ($\dot{x}_t - v > 0$): sliding contact with negative relative speed and positive friction force;
- Sticking ($\dot{x}_t = v$);
- Detachment ($x_n > 0$): no contact interaction between the mass and the slider.

These conditions can be reached independently on each contact between mass and slider; thus the system can reach 4^n possible combinations of the contact status, where n is the number of subsystems.

The simulations here reported are performed with the system composed by 2 subsystems (cf. Fig. 1) and the values of the system parameters, chosen in order to have two unstable modes for acceptable values of the friction coefficient, are reported in Table 1.

Parameter	Value
m_1, m_2	0.3 kg
m_3, m_4	0.7 kg
k_1	1.8e+6 N/m
k_2	4.5e+5 N/m
k_3	6.0e+4 N/m
k_4	3.0e+5 N/m
k_5	1.5e+6 N/m
k_6	2.4e+5 N/m
k_7	3.0e+4 N/m
k_8	1.8e+5 N/m
k_9	2.4e+6 N/m
β	1.0e-4 s
θ_1	0.3
θ_2	0.75

Table 1 Parameters adopted in the lumped model.

3 Complex eigenvalue analysis

To find the eigenmodes of the system the equilibrium position is accounted for. It is supposed that all the contacts are in sliding condition. In this case the motion is constrained in the direction normal to the slider. The reaction force N gives origin to a tangential force $\|T\| = \mu N$ whose orientation agrees with that of the rigid slider speed.

In sliding condition each subsystem has 3 DoFs. The Damping matrix is introduced as to be proportional to the stiffness matrix. If the friction coefficient is nil the modes of the system can be expressed solving the eigenvalue problem for the mass and stiffness matrices.

$$\lambda \mathbf{M}\boldsymbol{\psi} = \mathbf{K}\boldsymbol{\psi} \tag{2}$$

where $\lambda = \omega^2$ are the real eigenvalues of the system and $\boldsymbol{\psi}$ are the real eigenvectors that represent the modal shapes (cf. Fig. 2). These eigenvectors are orthogonal with respect to the mass $\mathbf{M}$, the stiffness $\mathbf{K}$ and the damping $\mathbf{C}$ matrix. In this case the system can be diagonalized and the response can be expressed as a modal superposition response.

When the friction coefficient is not zero, it produces an asymmetry on the system matrices. In this case, the eigenmodes of the system can be found by means of a complex modal analysis, which takes into account the asymmetry of the matrices. The system can be expressed in the state space as follows:

$$\begin{cases} \mathbf{M}\ddot{\boldsymbol{x}} + \mathbf{C}\dot{\boldsymbol{x}} + \mathbf{K}\boldsymbol{x} = \boldsymbol{F} \\ \mathbf{M}\dot{\boldsymbol{x}} - \mathbf{M}\dot{\boldsymbol{x}} = \mathbf{0} \end{cases} \longrightarrow \quad \mathbf{A}\dot{\mathbf{y}} + \mathbf{B}\boldsymbol{y} = \boldsymbol{Q} \tag{3}$$

where,

$$\mathbf{A} = \begin{bmatrix} \mathbf{C} & \mathbf{M} \\ \mathbf{M} & \mathbf{0} \end{bmatrix}, \; \mathbf{B} = \begin{bmatrix} \mathbf{K} & \mathbf{0} \\ \mathbf{0} & -\mathbf{M} \end{bmatrix}, \; \boldsymbol{y} = \begin{Bmatrix} \boldsymbol{x} \\ \dot{\boldsymbol{x}} \end{Bmatrix} \text{ and } \boldsymbol{Q} = \begin{Bmatrix} \boldsymbol{F} \\ \mathbf{0} \end{Bmatrix}. \tag{4}$$

Being $\mathbf{C}$ and $\mathbf{K}$ asymmetric also $\mathbf{A}$ and $\mathbf{B}$ are asymmetric and the following eigenvectors can be defined:

$$\lambda \boldsymbol{\upsilon}^T \mathbf{A} = -\boldsymbol{\upsilon}^T \mathbf{B} \tag{5}$$

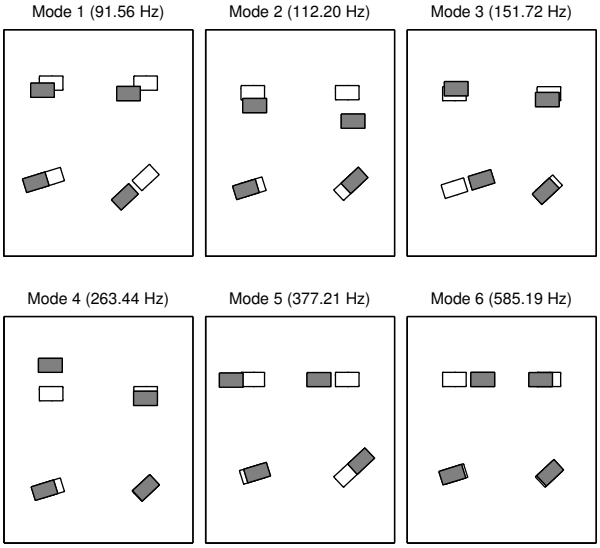

Fig. 2 Modal shapes in case of $\mu = 0$.

$$\lambda \mathbf{A}\boldsymbol{\xi} = -\mathbf{B}\boldsymbol{\xi} \tag{6}$$

where λ are in this case the complex eigenvalues and $\boldsymbol{\xi}$ and $\boldsymbol{\upsilon}$ are respectively the right and the left complex eigenvectors of the system. The matrices of the right complex eigenvectors $\boldsymbol{\Xi}$ and of the left complex eigenvectors $\boldsymbol{\Upsilon}$ allow to transform respectively the state variables and the forces, expressed in the state space, on the principal coordinates.

The eigenvalues can be expressed as a function of the angular frequency ω_i and the modal damping factor ζ_i of the i^{th} mode:

$$\lambda_i = -\omega_i \zeta_i + j\omega_i \sqrt{1-\zeta_i^2}. \tag{7}$$

The real part is correlated to the modal damping factor: a positive real part corresponds to modes with apparent negative modal damping factor (unstable modes). When the effects of friction forces increase (increase of the friction coefficient), eigenvalues having initially different frequency coalesce together (lock-in) and their real parts start to diverge (Hopf bifurcation point).

Figure 3 reports the trend of real and imaginary parts of each eigenvalue with respect to the friction coefficient μ. Eigenvalues at lower frequency are the first to coalesce for a critical friction coefficient $\mu_I = 0.7$. The two modes at higher frequency coalesce for a friction coefficient $\mu_{II} = 2.1$. It can be noticed that the positive real part of the lower eigenvalues overcome the real part of the higher eigenvalue for a friction coefficient between 0.7 and 2.4, while the opposite occurs for $\mu > 2.4$. Finally, two modes of the system are unstable if $\mu > 2.1$.

The calculated complex eigenvectors give information about both the relative amplitude of vibration and the initial phase of the vibration of each degree of freedom. Each

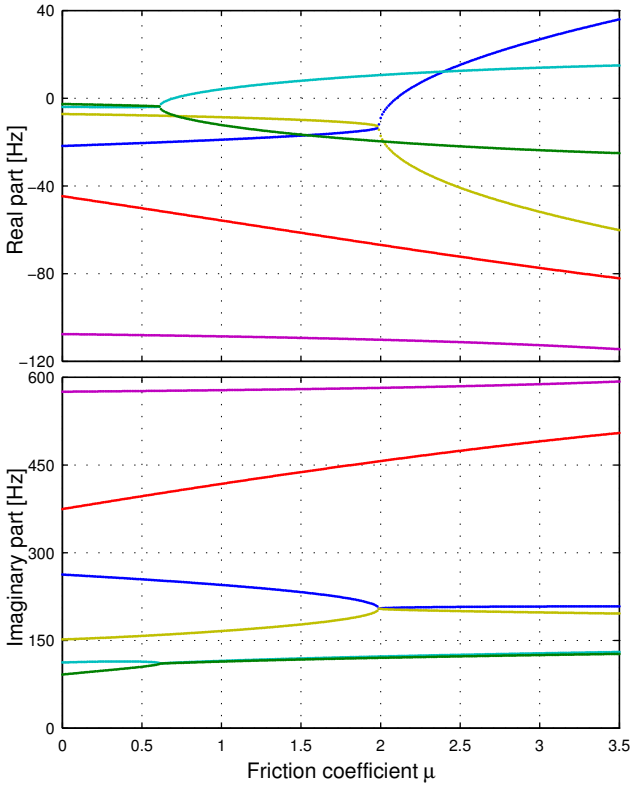

Fig. 3 Real and Imaginary part of the eigenvalues versus the friction coefficient

pair of complex conjugate modes gives the following (real) contribution to the solution in the state space:

$$\boldsymbol{y}_i(t) = \boldsymbol{\xi}_i e^{\lambda_i t} + \boldsymbol{\xi}_i^{\star} e^{\lambda_i^{\star} t}. \tag{8}$$

where the star symbol indicates the complex conjugate value. The complex eigenvectors have a length $2n$ where n is the number of DoF of the system. They are composed of two parts: the first part is related to the displacement and the second part is related to the speed $\boldsymbol{\xi}_i^T = \left\{ \boldsymbol{\psi}_i^T,\ \lambda_i \boldsymbol{\psi}_i^T \right\}$. Hence, the real contribution to the solution in the configuration space can be expressed as:

$$\begin{aligned} \boldsymbol{x}_i(t) &= \boldsymbol{\psi}_i e^{\lambda_i t} + \boldsymbol{\psi}_i^{\star} e^{\lambda_i^{\star} t} \\ &= 2e^{\lambda_{Ri} t} \left[\boldsymbol{\psi}_{Ri} \cos(\lambda_{Ii} t) - \boldsymbol{\psi}_{Ii} \sin(\lambda_{Ii} t) \right] \end{aligned} \tag{9}$$

where the R and I subscripts indicate respectively the real and imaginary part.

In complex modes the displacements of different DoFs of the system are in general neither in phase nor in phase opposition, even along the different degrees of freedom of the same mass.

The orbits of the masses of the system given by (9) allow for a physical interpretation of the different eigenvector pairs both in terms of vibration amplitude and in terms of the phase delay between the different DoFs of the system (Fig. 4).

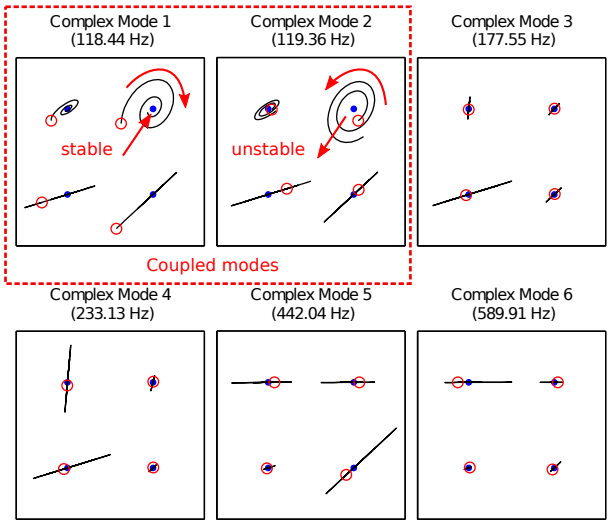

Fig. 4 Complex modal shapes for a friction coefficient $\mu = 1.5$. (○: initial point; ●: equilibrium position.)

Figure 4 shows the orbits for a friction coefficient $\mu = 1.5$. In this condition the system is characterized by one coupled mode at a frequency of 119 Hz (Modes 1 and 2 in Fig. 4). Convergent spirals correspond to stable modes while divergent spiral correspond to unstable modes. It can be noticed that for uncoupled modes there isn't any phase lag between the two orthogonal displacements of the same mass, and the orbit of each mass collapses on a segment. On the contrary, convergent or divergent spirals characterize the orbits of coupled modes. They indicate a phase lag between the two spatial DoFs of the same mass. Convergent spirals mean release of energy at each cycle of vibration, i.e. increase in the modal damping of the stable coalescing mode (decrease of the real part in Fig. 3); divergent spirals mean absorption of energy at each cycle of vibrations, i.e. decrease of the modal damping for the coalescing mode up to reach a negative value.

The displacement tangential and normal to the contact can be correlated respectively to the velocity and to the contact forces. The tangential speed is 90° ahead in phase with respect to the tangential position. On the contrary, the variations of the tangential and normal contact forces T and N are opposite in phase to the normal displacement of the upper mass. The power flow at the contact can be expressed as:

$$\widetilde{P}_c = \frac{1}{2}\mathrm{Re}\left[\underline{T}\,\underline{v}^{\star}\right] e^{2\lambda_R t} \tag{10}$$

where $\underline{T}$ is the tangential force phasor and $\underline{v}^{\star}$ is the complex conjugate phasor of the tangential velocity. Therefore, the phase lag between $\underline{T}$ and $\underline{v}^{\star}$, needed to compute the power flow, is directly related to the phase lag between the tangential displacement and the normal displacement of the upper mass. In conclusion, the phase lag between the normal and tangential displacement is related to the ability of each mode pair to absorb or release energy.

4 Transient non-linear analysis

When dealing with linear systems, the solution can be expressed as a linear combination of all the modes of the system. Basing on the real part of the eigenvalues, the system behavior can be stable or unstable.

For linear systems, if there are several unstable modes, the mode with greater real part of the eigenvalues grows exponentially faster than the others, and the contribution of the other modes becomes quickly irrelevant.

Real systems don't behave linearly because of the contact nonlinearities such as the change of contact status (stick, slip, detachment) or the nonlinear contact stiffness. When the vibration amplitude increases, the variation of the contact status (detachment or sticking) confines the exponential growth of the vibration amplitude. This is why the linear model is fully representative only of the initial part of this dynamic instability phenomenon. To simulate in a reliable way the whole transient analysis in the case of unstable friction induced vibrations, a non linear model is needed.

In this case the system can assume 4^n different status combinations. For each condition the complex eigenvalues and eigenvector can be computed. The response of the nonlinear system can be expressed as a sequence of linear responses. The nonlinearity of the system is related to the switching between the different contact status combinations.

The initial condition considered for simulation is the equilibrium position with all the contact masses in positive sliding and with a small perturbation on one DoF of the system. Left and Right eigenvalue problem are solved for all the masses of the system in the initial status and the response is calculated as modal superposition of a self-excited system.

During the transient response different scenarios can occur for each mass in contact: i) if the normal contact force reaches the nil value, the mass leaves the slider and passes to the detachment condition; ii) if the relative speed of the mass with respect to the slider reaches the nil value the system can either pass to the sticking status or overcome the nil value with the consequent inversion of relative motion (sign of the friction force).

For each combination of contact status of the contact masses a different set of differential equations can be written. Each time a switch condition is reached, the position in the state plane of the system becomes the initial condition of the new set of differential equations.

In sliding and detachment status the right member of (3) is composed by a constant term, that depends to the preloads (forces or displacements) applied to the system. Conversely in sticking status it is composed by a constant term and a

linear term, related to the increase of the elastic force with time. It can be generalized as:

$$\boldsymbol{Q} = \boldsymbol{Q_0} + \boldsymbol{Q_1} t. \tag{11}$$

The complex modal analysis introduced in section 3 can be useful to diagonalize the system. Considering the matrices $\boldsymbol{\Upsilon}$ and $\boldsymbol{\Xi}$ respectively of left and right eigenvectors defined in (5) and (6) is possible to transform the forces and displacements in the generalized coordinates $\boldsymbol{z}$:

$$\boldsymbol{y} = \boldsymbol{\Xi} \boldsymbol{z} \tag{12}$$

$$\boldsymbol{p} = \boldsymbol{\Upsilon}^T \boldsymbol{Q} \tag{13}$$

These two matrices result to be bi-orthogonal and the system can be diagonalized as follows:

$$\boldsymbol{\Upsilon}^T \mathbf{A} \boldsymbol{\Xi} \dot{\boldsymbol{z}} + \boldsymbol{\Upsilon}^T \mathbf{B} \boldsymbol{\Xi} \boldsymbol{z} = \boldsymbol{\Upsilon}^T \boldsymbol{Q} \tag{14}$$

$$\begin{bmatrix} \ddots & a_r & \ddots \end{bmatrix} \dot{\boldsymbol{z}} + \begin{bmatrix} \ddots & b_r & \ddots \end{bmatrix} \boldsymbol{z} = \boldsymbol{p_0} + \boldsymbol{p_1} t. \tag{15}$$

The time response in generalized coordinate is solution of (15). Finally, the response on the state space can be expressed for each contact configuration as follows:

$$\boldsymbol{y}(t) = \boldsymbol{\Xi} \begin{bmatrix} \ddots & e^{\lambda_r t} & \ddots \end{bmatrix} \boldsymbol{\Xi}^{-1} \boldsymbol{y}_0 + \boldsymbol{\Xi} \begin{bmatrix} \ddots & b_r & \ddots \end{bmatrix}^{-1} \begin{bmatrix} \ddots & 1 - e^{\lambda_r t} & \ddots \end{bmatrix} \boldsymbol{p}_0 + \\ + \boldsymbol{\Xi} \begin{bmatrix} \ddots & b_r & \ddots \end{bmatrix}^{-1} \begin{bmatrix} \ddots & \dfrac{1 - e^{\lambda_r t}}{\lambda_r} + t & \ddots \end{bmatrix} \boldsymbol{p}_1 \tag{16}$$

4.1 Transient response analysis

Figure 5 shows a typical behavior of the system when at least one of the modes is unstable. The system starts from its equilibrium position and the vibration amplitude increases exponentially until it reaches a stationary value. The stationary state is characterized by a limit cycle and is related to the occurrence of nonlinear transitions at the contact. Results here reported are referred to a friction coefficient $\mu = 1.5$: in this case, (cf. plot of the real part in Fig. 3) only one system mode is unstable. The initial perturbation is $\dot{x}_1(0) = 1\mathrm{e}-3\,\mathrm{m/s}$. The boundary conditions considered for this simulation are $v_{1,2} = 2.5\mathrm{e}-2\,\mathrm{m/s}$ and $\delta_{1,2} = 1\mathrm{e}-3\,\mathrm{m}$.

In the initial part of the simulation, when the system behaves linearly, the excited frequencies are the same calculated by the linear complex modal analysis (cf Fig. 3), due to the system instability and the initial perturbation. The perturbation affects the initial part of the response by exciting the system modes as a function of the perturbation "shape".

The mode with a shape that is more similar to the initial perturbation gives to the system response an initial larger contribution. On the contrary the steady state reached by the system is not at all affected by the initial perturbation, confirming that the harmonic content and the behavior of the system during the limit cycle is directly correlated to the system parameters. In Fig. 6 the state diagrams of the x_2 and x_6 coordinate highlight the limit cycle of the system.

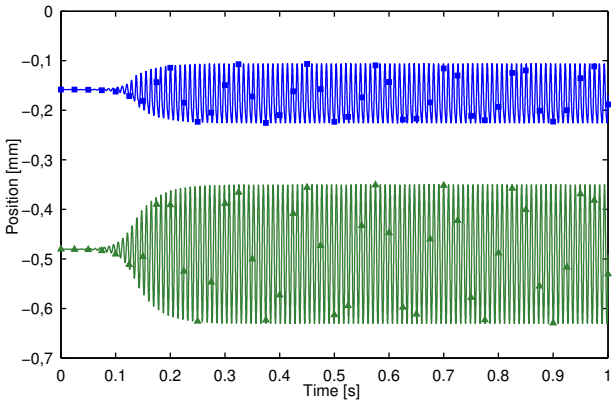

Fig. 5 Displacement response for a friction coefficient $\mu = 1.5$. (■ x_2; ▲ x_6)

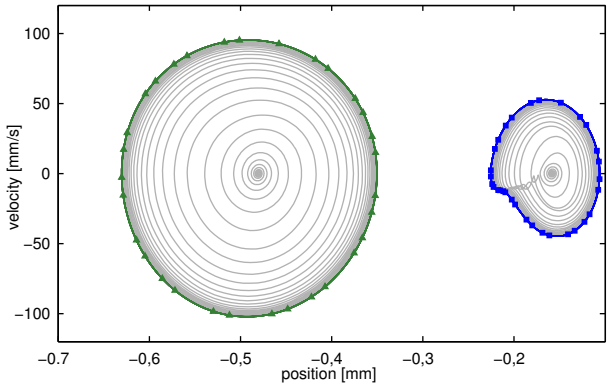

Fig. 6 State diagram of the system and the limit cycle. (■ DoF_2; ▲ DoF_6)

In this analysis the nonlinear response is expressed as a sequence of linear responses. For each combination of contact statuses it is possible to find the eigenvalues of the system and express the response as a modal superposition until the system switches in a new status. In this case the first subsystem alternate between sliding (Sl) and sticking (St) while the second subsystem alternates among sliding (Sl), detachment (Dt) and sticking (St) (cf. Fig. 7). During the limit cycle the whole system alternates among a sequence of 4 different combinations of contact statuses.

Table 2 shows the frequencies of the system for each configuration involved in the transient response. Results reported in Tab. 2 highlight that the system alternates in this case among two unstable contact status and two stable contact status.

The Fourier transforms of the response signal in Fig. 8 highlight the main frequencies that characterize the unsta-

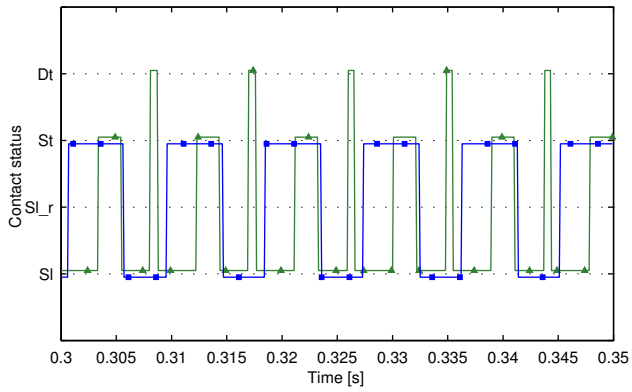

Fig. 7 Status of the two contacting mass on the limit cycle. (■ m_2; ▲ m_4)

	Contact Status			
	Sl - Sl	St - Sl	St - St	Sl - Dt
Freq. [Hz]	118.44	113.38	113.14	31.59
	119.35	125.40	258.47	116.15
	177.55	258.47	326.10	**116.60**
	233.13	306.51	582.02	173.77
	442.04	581.45	-	233.66
	589.90	-	-	418.60
	-	-	-	588.18

Table 2 Modal frequencies for the different configurations reached by the system during the simulation for a friction coefficient $\mu = 1.5$. Bold values indicate the unstable modes.

ble vibration. During the initial part of simulation, when the system is in sliding condition on both the contact masses, the vibration recovered is at a frequency that is the same of the unstable mode reported in the first column of Table 2. In this condition the system absorbs energy by the contact, increasing the energy content and consequently the vibration amplitude.

During the limit cycle the frequency recovered is 112 Hz. This frequency is not directly imputable to one of the modal

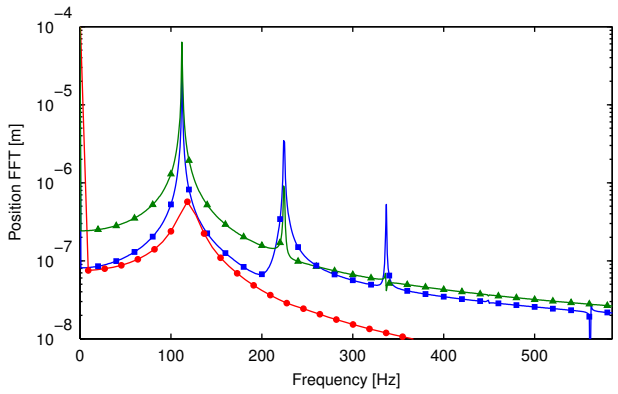

Fig. 8 Frequency content of the transient response during the initial part the response and during the limit cycle. (■: x_2 response in the limit cycle; ▲: x_6 response in the limit cycle; ●: x_2 response in the initial part $(0 < t < 0.11)$).

analysis reported in Table 2. The response is a sequence of different status combinations, each one characterized by a set of natural frequencies. This brings to a spectrum of the response characterized by a main harmonic, that is close to the frequency of the unstable mode, and its superharmonics, which appear with the appearing of the contact nonlinearities. Furthermore, during the limit cycle, the alternation between different contact conditions brings the system to switch between configuration of energy absorption and energy release, that are balanced during the period of the limit cycle. Thus, there is no variation of the energy content of the system and the vibration amplitude stabilizes at the limit cycle.

5 Effect of boundary conditions on the transient response

5.1 Effects of friction coefficient

With respect to the different behaviors of the system, highlighted by the parametric complex eigenvalue analysis, transient nonlinear simulations have been developed as a function of the friction coefficient (cf. Fig. 3). According to the critical friction coefficients introduced in section 3 the following ranges can be defined:

- $\mu < 0.70$: the system is stable;
- $0.70 < \mu < 2.1$: the system is unstable because one of the eigenvalue at lower frequency has a positive real part;
- $2.1 < \mu < 2.4$: the system is unstable and there are two eigenvalues at both lower and higher frequency with positive real part. The real part of the eigenvalue with lower frequency is larger;
- $\mu > 2.4$: the system is unstable because there are two eigenvalues at both lower and higher frequency with positive real part. The real part of the eigenvalue with higher frequency is larger.

In case of stable behavior of the system, the amplitude of vibration decreases with exponential decay. If the initial amplitude of vibration is less than the amplitude that brings to the contact status variation, the system behaves linearly and tends exponentially to reach its static equilibrium position.

In case of unstable behavior of the system, the amplitude of vibration, initially induced by a small perturbation, increases exponentially until the first mass in contact reaches one of the possible status variations. Then the exponential increase of the vibration amplitude stops and the system vibration reaches its limit cycle.

Figure 9 shows the Fourier transform of the position response signal for three different analyses, performed on the same model introduced in section 4.1, with three different values of the friction coefficient ($\mu_1 = 1.5$, $\mu_2 = 2.2$ and

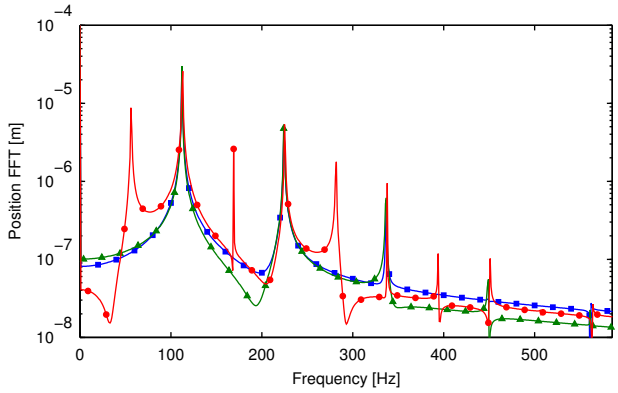

Fig. 9 Fast Fourier Transform of the response during the limit cycle for different friction coefficient. (■: $\mu_1 = 1.5$; ▲: $\mu_2 = 2.2$; ●: $\mu_3 = 3.0$).

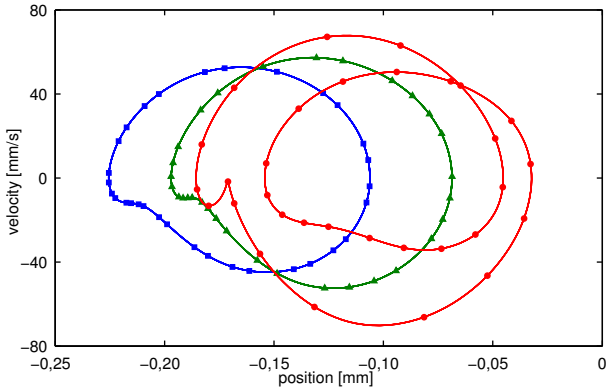

Fig. 10 Limit cycle of the DoF x_2 for different friction coefficient. (■: $\mu_1 = 1.5$; ▲: $\mu_2 = 2.2$; ●: $\mu_3 = 3.0$).

$\mu_3 = 3.0$). The friction coefficients chosen for this comparison are set to cover the three possible unstable conditions highlighted by the parametric complex eigenvalue analysis (cf. Fig. 3). The Fourier transforms show that the global response of the system is not affected by the variation of the real part of the eigenvalues. The harmonic content remains about the same for the two friction coefficients μ_1 and μ_2, even if in the second case two unstable modes are predicted by the CEA. For a friction coefficient μ_3 there are still the two unstable modes, but in this case the response is characterized by the subharmonics of the main frequency.

It is important to notice that the main frequency of the response remains the same (at about 112 Hz) in the three cases, even for the friction coefficient μ_3. This means that the unstable mode recovered during the transient response is not directly related to the value of the real part of the eigenvalues calculated by CEA. The selection mechanism of the unstable mode, when several modes result to have positive real part, cannot be predicted by the system eigenvalues and is rather related to the energy transfer associated with each mode. Moreover, results of complex modal analysis doesn't allow to express in a deterministic way the transient response, which is highly influenced by the contact nonlinearities and depends on other physical aspects such as the energy equilibrium during the periodic non linear response.

Figure 10 shows the trace on the state plane during the limit cycle. The different curves are referred to the same degree of freedom (x_2 in Fig. 1) for the different friction coefficients. This figure compared with Fig. 9 highlights that the limit cycle for the friction coefficient μ_1 and μ_2 are about the same, with a small variation of the vibration amplitude. For a friction coefficient μ_3 the subharmonic that appears in the Fourier transform (cf. Fig. 9) is associated to a double tour on the state plane in Fig. 10 that produce a doubling of the time period.

5.2 Effect of the slider velocity

Four different values of the slider speed ($v_1 = 2.5e-2$ m/s; $v_2 = 5.0e-2$ m/s; $v_3 = 3.0e-1$ m/s and $v_4 = 9e-1$ m/s) have been selected with the aim to obtain different sequence of contact status (cf. Table 3) and to observe how these variation can be related to different behaviors of the system. Increasing the speed of the sliders, the system reaches the detachment condition and other modes are involved into the response of the system. Table 3 shows all the contact status combinations obtained for the different velocities.

speed	**configurations**						
v_1	Sl Sl	St Sl	St St				
v_2	Sl Sl	Sl St	St Sl	St St	St Dt	Dt Sl	
v_3	Sl Sl	Sl St	Sl Dt	St Sl	St St	St Dt	Dt Dt

Table 3 Status configurations involved in the response for different value of the sliders speed.

Analyses here reported are referred to the same model with a friction coefficient $\mu = 2.2$. For this value of the friction coefficient, in sliding condition, the system is characterized by two unstable modes at the frequencies $f_1 = 124.1$ Hz and $f_2 = 206.4$ Hz. Table 4 shows the effects of contact status combinations on the eigenvalues of the system.

Figure 11 shows the Fourier transform of the response for different values of the slider speed. The main frequency recovered for these simulations is about the same and it is close to that of the first unstable mode.

The numbers of different statuses involved in the response increases with the plane speed. The sequence of different contact status combinations can produce small variations of the main frequency recovered during the limit cycle. The appearance and the relative amplitude of the sub-

Contact status of first mass	Contact status of second mass: Sl	St	Dt
Sl	122,93	130,46	31,64
	124,18	178,72	118,22
	204,11	212,87	**118,71**
	206,45	328,13	201,20
	468,96	584,23	**202,86**
	593,28	-	418,71
	-	-	588,25
	-	-	-
St	113,43	113,14	31,48
	132,05	258,47	113,55
	258,47	326,10	118,12
	467,78	582,02	258,48
	591,50	-	417,52
	-	-	586,23
	-	-	-
	-	-	-
Dt	68,78	68,71	30,58
	119,67	143,64	69,52
	143,61	149,87	109,80
	162,24	303,73	143,77
	303,73	327,84	157,82
	468,61	583,51	303,73
	592,69	-	418,38
	-	-	587,59

Table 4 Modal frequencies for the different configurations reached by the system during the simulation for a friction coefficient $\mu = 2.2$. Bold values indicate the unstable modes.

harmonics is related to the different combinations of contact statuses during the limit cycle.

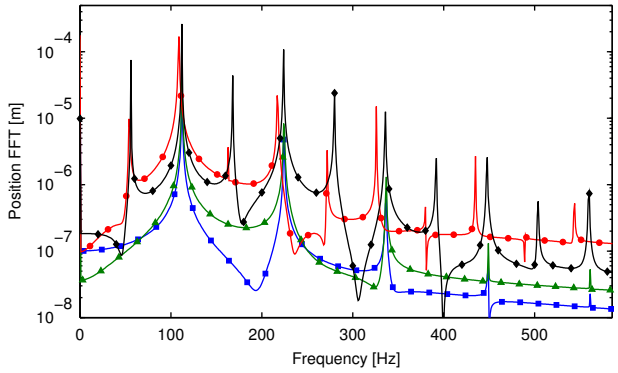

Fig. 11 Fast Fourier transform of the system response during the limit cycle. (■: $v_1 = 2.5e-2\,m/s$; ▲: $v_2 = 5.0e-2\,m/s$; ●: $v_3 = 3.0e-1\,m/s$ and ♦: $v_4 = 9e-1\,m/s$).

The variation of the slider speed produces evident results observing the state diagram. The amplitude of vibration increases with the increase of the speed. This is related to the excitation during sticking phases that are present for all the simulations. For the speed v_1 and v_2 the traces on the state plane are of the same shape with only a difference in amplitude. For higher speeds the shape of the trace on the state plane is different and characterized by a higher contribution of the subharmonics and superharmonics.

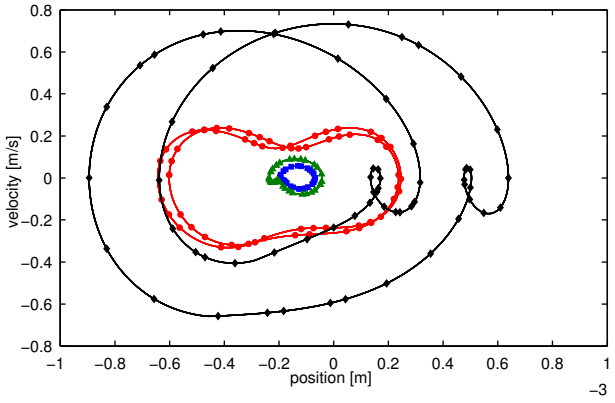

Fig. 12 Comparison of limit cycles for different speed of the contacting sliders. (■: $v_1 = 2.5e-2\,m/s$; ▲: $v_2 = 5.0e-2\,m/s$; ●: $v_3 = 3.0e-1\,m/s$ and ♦: $v_4 = 9e-1\,m/s$).

6 Energy analysis

At the contact, the system exchanges power P_c with the slider by means of the contact forces. Furthermore, the system exchanges power P_{Fex} with the external environment by means of the external forces F_{Ex}. The viscous damping dissipates the power P_m during the vibration. The derivative of the total mechanical energy can be expressed in this case as:

$$\frac{dE_t}{dt} = P_c(t) + P_{Fex}(t) - P_d(t). \tag{17}$$

The total energy can be decomposed into kinetic and potential terms and represents the energy stored by the system (cf. upper plot in Fig. 13).

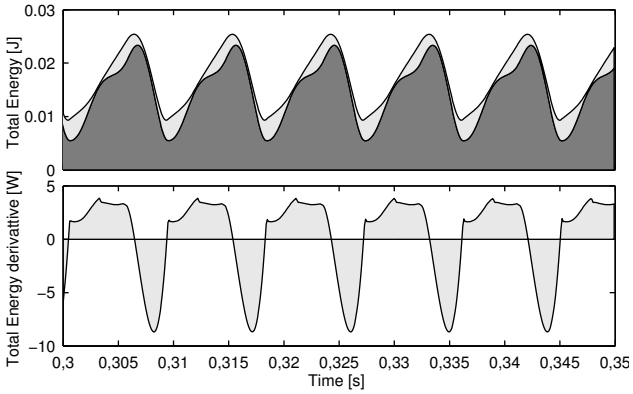

Fig. 13 Decomposition, during the limit cycle, of the E_t into Kinetic (light gray) and Elastic (dark gray) energy (up) and derivative of the total energy over the time dE_t/dt (down).

The fluctuation of the total energy is related to the energy balance expressed in (17).

Results presented in Fig. 13 refer to the same simulation analyzed in 4.1; comparing the contact status in Fig. 7 with

the total energy and its derivative in Fig. 13 the same period of oscillations can be observed.

Figure 14 shows the decomposition of the total energy derivative into the different power terms in (17). The comparison between this results and the transition among different configurations of contact (cf. Fig. 13), highlights that the system globally absorbs energy during the sticking condition of the first mass and releases energy during the sliding condition of the first mass. In the limit cycle the duration of these different phases is such that the energy absorbed and released by the system are balanced and they don't produce any variation of the total energy of the system during the cycle. This leads to have an amplitude of vibration constant in time (limit cycle).

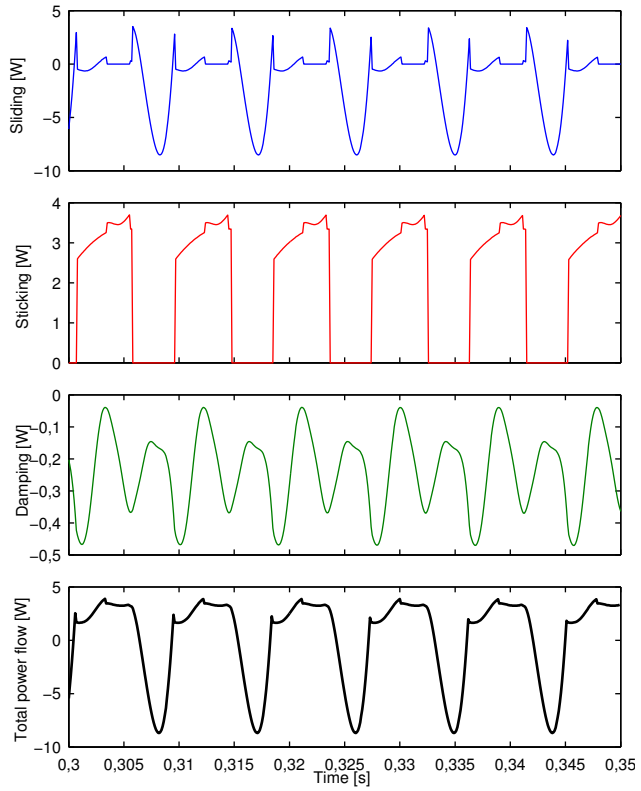

Fig. 14 Decomposition, during the limit cycle, of the dE_t into power exchanged throw the contact interface and dissipated by the damping.

Figure 15 shows the decomposition of the total energy derivative during the initial part of the same simulation, when the exponential increase of the unstable vibration amplitude brings the system to reach the first switches of the contact status. The total power oscillates and the power globally introduced into the system during a pseudo-period of vibration is positive. It is because the positive contribution prevails over the negative one before the beginning of cyclic variation of the contact configuration. In the last plot in Fig. 15 the variations of contact status occur when the total power flow is positive. This produces a limitation of the absorbed energy, that becomes equal to the released energy, and this equilibrium brings the system to the stationary state with the periodization of all the contact status switching.

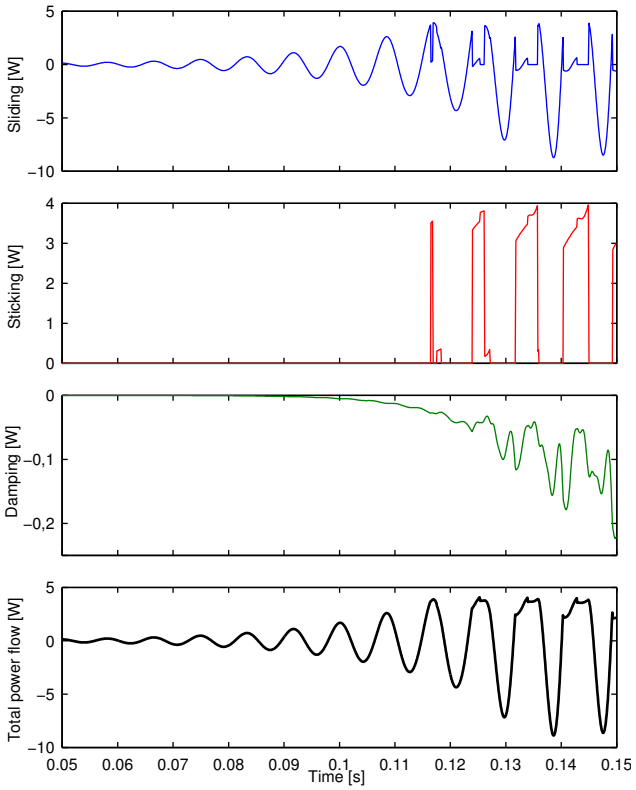

Fig. 15 Decomposition, during the initial part of the response, of the dE_t into power exchanged throw the contact interface and dissipated by the damping.

7 Conclusions

In this paper, the development and analysis on a lumped parameters nonlinear model, composed by several degrees of freedom, is presented. The presence of frictional contact allows for the system to be unstable. By a parametric complex modal analysis on the linearized model, the effects of the variation of the friction coefficient on the system stability have been highlighted. System configurations with either one or several unstable modes are recovered. The instability of the coalescing mode has been related to the relative phase between normal forces and tangential displacements at the contact, which governs the energy flow between the system and the contact. Divergent spirals on the orbits of the complex mode shapes characterize unstable modes, i.e. absorption of energy.

The nonlinear transient analysis has been expressed as a sequence of linear responses, considering all the possi-

ble contact status combinations between the masses and the sliders (switching between local sliding, sticking or detachment). By this way the limit cycle of the system has been found accounting for the contact nonlinearities. The effects of boundary conditions on the limit cycle of the system response have been analyzed. Results reported in this paper show that when the friction coefficient is in the instability range, the variation of its value produces a variation of the amplitude of the response. Nevertheless, the harmonic content of the response doesn't change substantially, even if the ranking of the real parts of the eigenvalues calculated by the complex modal analysis changes.

On the contrary, the variation of the slider velocity modifies the contact status during the limit cycle and relevant variations of the harmonic contents can be noticed by the appearance of the subharmonics.

The complex eigenvalue analysis performed for all the different combinations of the contact statuses allows for highlighting how the appearance of superharmonics and subharmonics of the unstable frequency is related to the periodical switch between the different configurations.

The analysis of the energy balance during the limit cycle of vibrations gives an energy interpretation of the bounding of the unstable vibration through the contact nonlinearities: the periodical switching between different contact configurations allows for an energy balance that brings to the constant amplitude of vibration at the limit cycle.

References

Akay A (2002) Acoustics of friction. The Journal of the Acoustical Society of America 111(4):1525–1548, DOI 10.1121/1.1456514

Baillet L, Linck V, D'Errico S, Laulagnet B, Berthier Y (2005) Finite element simulation of dynamic instabilities in frictional sliding contact. Journal of Tribology 127(3):652–657, DOI doi:10.1115/1.1866160

Bengisu M, Akay A (1994) Stability of friction-induced vibrations in multi-degree-of-freedom systems. Journal of Sound and Vibration 171(4):557 – 570, DOI http://dx.doi.org/10.1006/jsvi.1994.1140

Brunetti J, Massi F, Saulot A, D'Ambrogio W (2013) Modal dynamic instabilities generated by frictional contact. In: Proceedings of the 5th World Tribology Congress (WTC-2013)

Brunetti J, Massi F, Saulot A, Renouf M, D'Ambrogio W (2014) System dynamic instabilities induced by sliding contact: a numerical analysis with experimental validation. Mechanical Systems and Signal Processing [submitted] -:–

Cantone F, Massi F (2011) A numerical investigation into the squeal instability: Effect of damping. Mechanical Systems and Signal Processing 25(5):1727 – 1737, DOI http://dx.doi.org/10.1016/j.ymssp.2010.12.005

Chen G, Zhou Z (2007) A self-excited vibration model based on special elastic vibration modes of friction systems and time delays between the normal and friction forces: A new mechanism for squealing noise. Wear 262:1123 – 1139, DOI http://dx.doi.org/10.1016/j.wear.2006.11.014

Chevillot F, Sinou JJ, Hardouin N, Jézéquel L (2010) Effects of damping on the speed of increase and amplitude of limit cycle for an aircraft braking system subjected to mode-coupling instability. Archive of Applied Mechanics 80(9):1045–1054, DOI 10.1007/s00419-009-0352-8

Coudeyras N, Sinou JJ, Nacivet S (2009) A new treatment for predicting the self-excited vibrations of nonlinear systems with frictional interfaces: The constrained harmonic balance method, with application to disc brake squeal. Journal of Sound and Vibration 319(3):1175 – 1199, DOI http://dx.doi.org/10.1016/j.jsv.2008.06.050

Dezi M, Forte P, Frendo F (2014) Motorcycle brake squeal: experimental and numerical investigation on a case study. Meccanica 49(4):1011–1021, DOI 10.1007/s11012-013-9848-y, URL http://dx.doi.org/10.1007/s11012-013-9848-y

Di Bartolomeo M, Massi F, Baillet L, Culla A, Fregolent A, Berthier Y (2012) Wave and rupture propagation at frictional bimaterial sliding interfaces: From local to global dynamics, from stick-slip to continuous sliding. Tribology International 52(0):117 – 131, DOI http://dx.doi.org/10.1016/j.triboint.2012.03.008

Fan N, Chen G, Qian L (2011) Analysis of squeaking on ceramic hip endoprosthesis using the complex eigenvalue method. Wear 271(9-10):2305 – 2312, DOI http://dx.doi.org/10.1016/j.wear.2010.12.024, 18th International Conference on Wear of Materials

Giannini O, Sestieri A (2006) Predictive model of squeal noise occurring on a laboratory brake. Journal of Sound and Vibration 296(3):583 – 601, DOI http://dx.doi.org/10.1016/j.jsv.2006.02.022

Hoffmann N, Gaul L (2003) Effects of damping on mode-coupling instability in friction induced oscillations. ZAMM - Journal of Applied Mathematics and Mechanics 83(8):524–534, DOI 10.1002/zamm.200310022

Hoffmann N, Fischer M, Allgaier R, Gaul L (2002) A minimal model for studying properties of the mode-coupling type instability in friction induced oscillations. Mechanics Research Communications 29(4):197 – 205, DOI http://dx.doi.org/10.1016/S0093-6413(02)00254-9

Ibrahim RA (1994a) Friction-induced vibration, chatter, squeal, and chaos - part i: Mechanics of contact and friction. Applied Mechanics Reviews 47(7):209–226, DOI doi: 10.1115/1.3111079

Ibrahim RA (1994b) Friction-induced vibration, chatter, squeal, and chaos - part ii: Dynamics and modeling. Applied Mechanics Reviews 47(7):227–253, DOI doi: 10.1115/1.3111080

Kinkaid N, O'Reilly O, Papadopoulos P (2003) Automotive disc brake squeal. Journal of Sound and Vibration 267(1):105 – 166, DOI http://dx.doi.org/10.1016/S0022-460X(02)01573-0

Massi F, Giannini O (2008) Effect of damping on the propensity of squeal instability: An experimental investigation. The Journal of the Acoustical Society of America 123(4):2017–2023, DOI 10.1121/1.2875628

Massi F, Giannini O, Baillet L (2006) Brake squeal as dynamic instability: An experimental investigation. The Journal of the Acoustical Society of America 120(3):1388–1398, DOI 10.1121/1.2228745

Massi F, Baillet L, Giannini O, Sestieri A (2007) Brake squeal: Linear and nonlinear numerical approaches. Mechanical Systems and Signal Processing 21(6):2374 – 2393, DOI http://dx.doi.org/10.1016/j.ymssp.2006.12.008

Ouyang H, Nack W, Yuan Y, Chen F (2005) Numerical analysis of automotive disc brake squeal: a review. International Journal of Vehicle Noise and Vibration 1(3-1):207–231, DOI doi:10.1504/IJVNV.2005.007524

Renouf M, Massi F, Saulot A, Fillot N (2011) Numerical tribology of dry contact. Tribology International 44(7-8):834–844

Sheng G (2007) Friction-Induced Vibrations and Sound: Principles and Applications. CRC, DOI ISBN-13: 978-1420051797

Sinou JJ, Jézéquel L (2007) Mode coupling instability in friction-induced vibrations and its dependency on system parameters including damping. European Journal of Mechanics - A/Solids 26(1):106 – 122, DOI http://dx.doi.org/10.1016/j.euromechsol.2006.03.002

Sinou JJ, Thouverez F, Jézéquel L (2004) Methods to reduce non-linear mechanical systems for instability computation. Archives of Computational Methods in Engineering 11(3):257–344, DOI 10.1007/BF02736228

Tonazzi D, Massi F, Culla A, Baillet L, Fregolent A, Berthier Y (2013) Instability scenarios between elastic media under frictional contact. Mechanical Systems and Signal Processing 40(2):754 – 766, DOI http://dx.doi.org/10.1016/j.ymssp.2013.05.022

Weiss C, Hothan A, Huber G, Morlock MM, Hoffmann NP (2012) Friction-induced whirl vibration: Root cause of squeaking in total hip arthroplasty. Journal of Biomechanics 45(2):297 – 303, DOI http://dx.doi.org/10.1016/j.jbiomech.2011.10.025

A System matrices in sliding condition

With reference to the system in Fig. 1 the system matrices used in (3) to solve the complex eigenvalue problem can be defined writing the Lagrangian equation of the system to find the equation of motion considering the normal and tangential forces at the contact.

Applying the sliding condition on both the contacting points:

$$\begin{cases} x_4 = \dot{x}_4 = \ddot{x}_4 = 0 & \text{and} \quad T_1 = \mu N_1 \\ x_8 = \dot{x}_8 = \ddot{x}_8 = 0 & \text{and} \quad T_2 = \mu N_2 \end{cases} \tag{18}$$

the number of DoFs of the system can be reduced up to 6.

The coordinate vector of the system is in this case:

$$\boldsymbol{x} = \begin{bmatrix} x_1 & x_2 & x_3 & x_5 & x_6 & x_7 \end{bmatrix}^T \tag{19}$$

and the mass and stiffness matrices are:

$$\mathbf{M} = \operatorname{diag}\left(\begin{bmatrix} m_1 & m_1 & m_2 & m_3 & m_3 & m_4 \end{bmatrix}\right) \tag{20}$$

$$\mathbf{K} = \begin{bmatrix} k_1+k_3+k_8 & 0 & -k_8a_1 \\ 0 & k_2+k_5+k_6 & -k_2b_1 \\ -k_8(a_1+\mu b_1) & k_2(\mu a_1-b_1) & k_8a_1^2+k_2b_1^2+\mu(k_8-k_2)a_1b_1 \\ -k_3 & 0 & 0 \\ 0 & -k_6 & 0 \\ 0 & 0 & 0 \end{bmatrix}$$

$$\begin{bmatrix} -k_3 & 0 & 0 \\ 0 & -k_6 & 0 \\ 0 & 0 & 0 \\ k_3+k_9 & 0 & -k_9a_2 \\ 0 & k_4+k_6+k_7 & -k_4b_2 \\ -k_9(a_2+\mu b_2) & k_4(\mu a_2-b_2) & k_9a_2^2+k_4b_2^2+\mu(k_9-k_4)a_2b_2 \end{bmatrix} \tag{21}$$

where:

$$a_i = \cos\theta_i \quad \text{and} \quad b_i = \sin\theta_i \tag{22}$$

The damping matrix is defined as proportional to the stiffness matrix by means of the proportional coefficient β defined in Table 1:

$$\mathbf{C} = \beta\mathbf{K} \tag{23}$$

Finally, the forces vector at the second member of (3) assumes the following value:

$$\boldsymbol{F} = \begin{bmatrix} 0 & -k_5\delta_1 - F_{Ex,1} & 0 & 0 & -k_7\delta_2 - F_{Ex,2} & 0 \end{bmatrix}^T \tag{24}$$

The same approach can be applied for each contact condition.